# Hidden Symmetry-Broken Phase of $MoS_2$ Revealed as A Superior Photovoltaic Material

Meiling Xu[†,ξ], Yue Chen[*,‡], Fen Xiong[‡], Jianyun Wang[†], Yanhui Liu[§], Jian Lv[†], Yanchao Wang[*,†,‡], Zhongfang Chen[&], and Yanming Ma[*,†,#]

[†]State Key Lab of Superhard Materials, College of Physics, Jilin University, Changchun 130012, China

[ξ]School of Physics and Electronic Engineering, Jiangsu Normal University, Xuzhou 221116, China

[‡]Department of Mechanical Engineering, The University of Hong Kong, Pokfulam Road, Hong Kong SAR

[§]Department of Physics, College of Science, Yanbian University, Yanji 133002, China

[&] Department of Chemistry, University of Puerto Rico, Rio PiedrasCampus, San Juan, PR 00931, USA

[#] International Center of Future Science, Jilin University, Changchun 130012, China

**Corresponding Authors:**

[*] **E-mail: yuechen@hku.hk**

[*] **E-mail: wyc@calypso.cn**

[*] **E-mail: mym@calypso.cn**

## Abstract

Monolayer $MoS_2$ has long been considered as the most promising candidate for wearable photovoltaic devices. However, its photovoltaic efficiency is restricted by its large band gap (2.0 eV). Though the band gap can be reduced by increasing number of layers, the indirect band gap nature of the resulting multilayer $MoS_2$ is unfavorable. Herein, we report a theoretical discovery of the hitherto unknown symmetry-broken phase (denoted as $1T_d$) of monolayer $MoS_2$ through a swarm structure search. The $1T_d$ phase has a distorted octahedral coordinated pattern of Mo, and its direct band gap of 1.27 eV approaches the optimal value of 1.34 eV that gives Shockley-Queisser limit for photovoltaic efficiency. Importantly, the direct band gap nature persists in thin films with multilayers owing to extremely weak vdW forces between adjacent $1T_d$ layers. The theoretical photovoltaic efficiency at 30 nm thickness reaches ~33.3%, which is the highest conversion efficiency among all the thin-film solar cell absorbers known thus far. Our results also demonstrate that proper electron injection is a practical route for experimental synthesis of the $1T_d$ phase. Once synthesized, the superior photovoltaic property of the $1T_d$ phase may lead to the development of an entirely new line of research for transition metal dichalcogenides solar cells.

Keywords: nanomaterials, $MoS_2$, energy harvesting, photovoltaics

## Introduction

The efficient use of solar energy, one of the most important forms of renewable energy, provides a potential solution to solve the energy and environmental challenges facing the world. Various solar energy devices have been developed in the past decade, such as silicon-based, dye-sensitized, and perovskite solar cells. However, these devices often have bulky structures. Unique optoelectronic properties and chemical robustness of layered structures, two-dimensional (2D) transition metal dichalcogenides (TMDs) have many applications in optoelectronics[1–3], catalysis[4–9], spintronics, and valleytronics[10,11]. Especial for $MoS_2$, it provides us new opportunities to develop portable, flexible, and wearable solar cells[12] as 2D solar cell material due to its high absorption coefficient ($10^7$ $m^{-1}$)[13–16].

Monolayer $MoS_2$ has three experimentally known polymorphs characterized by different coordination modes between Mo and S atoms, namely 1H, 1T and 1T'.[17] The 1H phase is most stable under normal conditions and is semiconducting, in which Mo adopts a trigonal prismatic coordination with S atoms. The 1T phase is characterized by the distorted layers and the octahedral coordination of Mo atoms, this metastable layer can made via intercalation of 1H-$MoS_2$ lattice with alkali metals. The distortion of 1T phase with the formation of Mo−Mo metal bonds gives rise to the 1T′ phase. Encouragingly, Zhang and coworkers just realized large-scale preparation of micrometre-sized metallic-phase 1T′-$MoS_2$-layered bulk crystals in high purity.[18] 1T and 1T' phases are either metallic or large-gap quantum spin Hall insulator[19], thus are hardly useful in terms of photovoltaic applications. Very recently, Du and coworkers theoretically predicted the not-yet-synthesized T" phase of $MoS_2$, which shows an intrinsic quantum spin Hall effect with a nontrivial gap and exhibits a topological phase transition driven by a small tensile strain.[20]

Monolayer $MoS_2$ in 1H phase (denoted as 1H-$MoS_2$) with only ~0.65 nm shows a large absorption coefficient of $10^7$ $m^{-1}$ comparable to that of commercialized 50nm-thick Si or 15nm-thick GaAs[12], which makes it useful for wearable photovoltaic applications. However, the band gap (~2.0 eV) of monolayer 1H-$MoS_2$ is too large to give an ideal Shockley-Queisser absorption efficiency (33.7%) that requires an optimal band gap value of ~1.34 eV. As a result, monolayer 1H-$MoS_2$ can only absorb incident sunlight up to 5−10% in the visible wavelength region[21]. The fabrication demands and the physics of the absorption efficiency suggest that multilayer $MoS_2$ may be more attractive than single layer $MoS_2$ for photovoltaic applications since thin film has a much-reduced band gap. It has been reported that 300-nm film of $MoS_2$ can absorb up to 95% of the light [22]. Unfortunately, the major drawback of the $MoS_2$ thin film is the indirect nature of its band gap[3] where phonons are required to mediate electron excitations from light. Then, a question raises naturally: is there a new phase of $MoS_2$ monolayer with high experimental feasibility and a direct and smaller band gap in the range of 1-1.5 eV?

We here report a theoretical discovery of the hitherto unknown monolayer phase of $MoS_2$ (donated

as $1T_d$) by carrying out the swarm-intelligence based CALYPSO structure searches. This $1T_d$ monolayer is semiconducting with a direct band gap of 1.27 eV. More importantly, the direct band gap nature persists in the thin film due to the extremely weak vdW interactions in the multilayer structures of $1T_d$ phase. The theoretical photovoltaic efficiency of $1T_d$ phase reaches ~33.3% at only 30 nm thickness, which is even higher than that of ~200-nm-thick GaAs (~32.0%) and far beyond that of the conventional 1H phase (19.0%). Our results also demonstrate that $1T_d$ phase could be synthesized by a proper electron injection method. Once synthesized, the superior photovoltaic property of $1T_d$-$MoS_2$ may open up an entirely new line of research for enhancing the efficiency of transition metal dichalcogenides (TMDCs) solar cell.

## COMPUTATIONAL METHODS

Structure searches of monolayer $MoS_2$ were carried out with simulation cells of up to 18 atoms using the swarm-intelligence based CALYPSO method[23–27], which has been benchmarked on various known systems, ranging from elements to binary and ternary compounds.[28–33] The population size was set to 100 and the structure search was terminated after the generation of up to 1,000 structures for each run. Structural optimizations, electronic structures, phonons, and molecular dynamics were performed in the framework of density functional theory (DFT). The generalized gradient approximation (GGA) expressed by PBE functional[34] as implemented in the Vienna Ab initio Simulation Package(VASP)[35] was adopted unless otherwise stated. The electron-ion interaction was described by the projector augmented-wave potentials[36], with $4p^6 4d^5 5s^1$ and $3s^2 3p^4$ configurations treated as the valence electrons of Mo and S, respectively. A kinetic cutoff energy of 500 eV and Monkhorst-Pack *k*-mesh sampling of 12×12×1 were adopted to ensure well converged total energies (~1 meV/atom). The ionic positions were fully relaxed until the residual force acting on each ion was less than 0.01 eV/Å. Sufficient vacuum was used along *z* direction i.e. perpendicular to the 2D sheet, to avoid spurious interaction among the periodic images. The dynamic stability of the predicted new phases was verified from phonon calculation using the direct supercell method as implemented in the PHONOPY code[37,38]. Ab initio molecular dynamic (AIMD) simulations were performed with the Nosé-Hoover thermostat to confirm the thermal stability. To evaluate the photovoltaic performance, we calculated the theoretical photovoltaic efficiency[39], which captures the band gap, shape of absorption spectrum and material-dependent non-radiative recombination loss.

Note that the standard GGA tends to underestimate the band gaps, thus for $MoS_2$ monolayers, we also employed Heyd−Scuseria−Ernzerhof (HSE) hybrid functional[40], which was proven to be a reliable method for the calculation of electronic structures, to evaluate the band gap values. However, for multilayer $MoS_2$ systems, both structural optimizations and band structure computations were carried out by standard PBE functional, since such an approach can well reproduce the experimental band gap values of multilayer $MoS_2$ due to the error cancellation (PBE substantially overestimates

the interlayer lattice parameter, thereby increasing the band gap), as recently demonstrated by Peelaers and Van de Walle[41].

## RESULTS AND DISCUSSION

Through CALYPSO structure searching simulations, the known phases including 1H, 1T, 1T′ and 1T" -$MoS_2$ have been successfully reproduced, demonstrating the reliability of our methodology in application to $MoS_2$. Importantly, our structural searches identified two unknown low-lying phases with $P31m$ and $P2/c$ symmetries (Fig. 1a and Table S1), denoted as $1T_d$-$MoS_2$ and 1H′-$MoS_2$, respectively. $1T_d$ structure can be obtained by distorting the octahedral coordination patterns of Mo atoms in 1T phase, while 1H′ phase can be viewed as re-organization of the unit cells of 1H phase (see the red dotted rectangle frame in Fig. 1). 1H' phase is slightly lower in energy than 1T phase (by 38 meV/f.u.). Remarkably, $1T_d$ phase is energetically more favorable than the known 1T and 1T′ phases by ~300 and 12 meV/f.u. (Fig. 1b), respectively. Moreover, no imaginary phonons have be found in the Brillouin zone of the newly discovered $1T_d$ and 1H′ phases (Fig. S1), providing direct evidence for their dynamical stability. Furthermore, our AIMD simulations showed that $1T_d$ phase does not suffer significant structural destruction at the end of 5ps simulation time at 600K (Fig. S2). The decent thermal stability also ensure its potential application in photovoltaics. Considering the relative high energy of the 1H' phase and its narrow band gap of 0.34 eV (by HSE functional, Fig. S1c), we will only focus on $1T_d$ phase in this work.

Interestingly, $1T_d$ phase has a direct band gap of 1.27 eV at the HSE level of theory (Fig. 2a). The dominant contributions to the highest occupied and the lowest unoccupied states are mainly from the *d* orbitals of Mo atoms. Comparing the geometric and electronic structures of $1T_d$ and 1T phases, we can find that a subtle change in crystal structure leads to a dramatic difference in the electronic properties: 1T phase, in which the S atoms are in octahedral coordination with Mo atoms, is metallic, whereas $1T_d$ phase, in which the S octahedral coordination is only slightly distorted, becomes semiconducting.

The electronic structures of TMDCs strongly depend on the coordination environments of the transition metals and its *d*-electron count, which gives rise to different electronic properties[42]. For $MoS_2$, Mo is a divalent ion and has a $d^2$ electron count. In both 1T and $1T_d$ phases, the non-bonding *d* states are located within the gap between the bonding ($\sigma$) and antibonding ($\sigma^*$) states (Fig. 2b, Fig. S3). Distorted octahedral coordination of Mo atoms in $1T_d$ phase leads to its lower symmetry ($C_{3v}$) compared with that of 1T phase ($O_h$). According to the ligand field theory[43], there are two degenerated $e_g$ and $t_{2g}$ orbitals in octahedrally coordinated structures with $O_h$ symmetry: the doubly degenerated $e_g$ orbitals contain $d_{z^2}$ and $d_{x^2-y^2}$ orbitals, and the triply degenerated $t_{2g}$ orbitals contain $d_{xy}$, $d_{yz}$, and $d_{xz}$ orbitals. Since the energy level of $t_{2g}$ is lower than that of $e_g$, the occupancy of two *d* electrons of Mo in the three-fold degenerated $t_{2g}$ orbitals lead to partially filled *d* orbitals, resulting in the metallic character of 1T phase. On the other hand, the *d* orbitals of Mo with $C_{3v}$ symmetry in $1T_d$

phase splits into one-fold $a_1$ orbital corresponding to $d_{z^2}$ orbital and two doubly degenerated $e$ orbitals corresponding to $d_{x^2-y^2}$, $d_{xy}$, $d_{xz}$, and $d_{yz}$ orbitals. Full occupation of one-fold $a_1$ orbitals by two Mo electrons defines the semiconducting behavior of $1T_d$ phase.

We further examined the band structures of $1T_d$ phase of $MoS_2$ with different thickness. At HSE level of theory, both the bilayer and the bulk $MoS_2$ keep the direct band-gap nature of the monolayer. The bulk has a gap of 1.36 eV, very close to the monolayer (1.27 eV) and bilayer (1.25 eV). The same trend persists when more mutltilayers are examined by BPE functional. At PBE level of theory, the multilayers (with layer numbers of 2, 4, and 6) and the bulk all remain the direct band-gap nature, and their band gap values change very little (in the range of 0.68 eV-0.76 eV, compared with 0.83 eV for the monolayer, Fig. 2c). These computations indicate that thinning the bulk $1T_d$ phase of $MoS_2$ down to the monolayer does not enhance the quantum confinement of electrons. This is in stark contrast to 1H phase of $MoS_2$, where a transition from direct to indirect band structure occurs as the number of layers increases.[3,44] This difference might result from the much weaker vdW interactions in the multilayer structures of $1T_d$ phase. As shown in Fig. 2d, the adjacent layers in $1T_d$ phase only have a coupling energy of 8.67 meV/f.u., much smaller than that in 1H phase (112 meV/f.u.). We also chosen the tri-layer $1T_d$ phase to examine the effect of the different stacking configurations, and found that the total energies and band structures for different stacking patterns are rather similar (Fig. S4). Thus, it is the extremely weak vdW forces between adjacent $1T_d$ layers that lead to the layer number independent geometric and electronic properties of $1T_d$ phase.

For a practical solar cell, the theoretical photovoltaic efficiency relies on the thickness of the absorber layer. Thus, we calculated the photovoltaic efficiencies of $1T_d$ $MoS_2$ absorber layers as a function of the thickness (Fig. 3) by taking the absorption coefficient and the thickness of absorber layer into consideration.[39] The same computations were performed for 1H $MoS_2$ layers and GaAs layers for comparison. Evidently, the $1T_d$ $MoS_2$ exhibits much higher photovoltaic efficiencies than 1H $MoS_2$ and GaAs for any given thickness. More importantly, $1T_d$ $MoS_2$ layers achieve high efficiencies with very thin absorber layers. For example, 30-nm-thick $1T_d$ $MoS_2$-based cells can have a photovoltaic efficiency up to 33.3%, in stark contrast, only when the thickness of absorbers is about 200 nm can the high efficiency of ~30.0% in GaAs be achieved.[45-47]

It was recently reported that metastable monolayer TMDCs can be obtained by chemical lithium intercalation[6] and electrostatic-doping[48]. Therefore electron injection may be a practical route to synthesize the newly predicted metastable phases. To evaluate the effects of electron filling on phase stability, we constructed a model system, in which all Mo atoms are replaced by electron richer Tc or Ru atoms. It is found that the $1T_d$ phases of $TcS_2$ and $RuS_2$ are energetically more favorable than the corresponding 1H phases (see Fig. 4a), suggesting that the $1T_d$ phase of $MoS_2$ may be obtained by adding one extra electron per unit cell. For comparison, two extra electrons per unit cell[49] are required to obtain the 1T phase of $MoS_2$ since only the 1T phase of $RuS_2$ is energetically favorable

than the 1H phase. Therefore, the experimental synthesis of $1T_d$ phase should be more accessible in view of the fewer extra electrons needed. In fact, distorted 1T superstructures have already been observed in experiments[50]; these superstructures may be closely related to our predicted $1T_d$ phase. In addition, we found that there is a large energy barrier of ~0.20 eV/atom (equivalent to ~2308 K) between the metastable $1T_d$ phase and the energetically most favorable 1H phase (see Fig. 4b). Therefore, the $1T_d$ phase will be kinetically protected once synthesized.

Our phonon dispersion computations showed that the free-standing 1T phase has two imaginary phonon modes at A (-1/3 1/3 0) and M point (0 1/2 0) (see the inset of Fig. 4c), signifying its decisive role in characterizing phase transitions. To confirm this, we produced the distorted structures by freezing the amplitudes of the atomic displacements along the normal coordinates of the softening phonon, then calculated the total energies for a series of atomic displacements along the vibrations corresponding to the A and M points while maintaining the rest of the structural parameters at the referenced structure values (see Fig. 4c). As expected, the $1T_d$ and 1T′ phases were identified during our structural optimizations. Since the $1T_d$ structure is energetically more favorable than 1T′, there is a higher possibility that the freestanding 1T phase eventually transforms to the $1T_d$ phase, which was confirmed by our AIMD simulations: the freestanding 1T-$MoS_2$ phase would undergo a spontaneous distortion, leading to the $1T_d$ phase at low temperature (300 K); however, $1T_d$ phase can only transform into 1T phase at 1000 K (Fig. S5). These findings demonstrate a feasible approach for active control of the experimental realization of $1T_d$ phase from experimentally synthesized 1T phase. To assist the future experimental characterization, we simulated the occupied state STM images at a bias of -0.5 V for the 1H, 1T, $1T_d$ and 1T′ $MoS_2$ (Fig. S6). Note that our simulated STM images of 1H phase[51] and 1T' phase[18] well agree with experiments.

Furthermore, we investigated five other $1T_d$-$MX_2$ monolayers: $MoSe_2$, $MoTe_2$, $WS_2$, $WSe_2$ and $WTe_2$. By comparing the energies of the $1T_d$-, 1T-, 1T'- and 1H-phases (Fig. S7), we found that all $1T_d$ phases are energetically more favorable than the 1T phases, though 1T' is the lowest-energy phase for all these TMD monolayers. Interestingly, all the $1T_d$-$MX_2$ are semiconductors with direct band gaps in the range of 1.10-1.34 eV at the HSE06 level of theory (Fig. S8). Their suitable band gaps endow $1T_d$ phase with potential applications in solar cells.

## Conclusion

In summary, a new semiconducting phase ($1T_d$) of monolayer $MoS_2$ with an optimal, direct optical band gap of 1.27 eV is discovered by the global optimization swarm intelligence algorithm. Thermodynamically this newly predicted monolayer is slightly more favorable than the recently synthesized 1T' phase. Due to the rather weak interlayer interactions, the geometric and electronic properties of $1T_d$ phase is nearly independent of layer number, especially its direct band gap nature persists in multilayers, and the band gap values can be slightly tuned by controlling the layer number.

The photovoltaic efficiency of the $1T_d$ phase reaches ~33.3%, which is close to the Shockley–Queisser limit, at only ~0.3 μm thickness. Our computations also suggest that it is highly promising to synthesize the $1T_d$ phase by electron injection, and it is also feasible to convert the experimentally synthesized 1T phase to $1T_d$ phase by proper annealing. Once synthesized, the superior photovoltaic property of the $1T_d$ phase may open a door to further exploring new high-performance TMD-based solar cells.

**Supporting Information**

Crystallographic Data of $1T_d$ and 1H′ phases; phonon dispersions and the band structures calculated from HSE06 functional of 1H′ phase; the AIMD simulations of $1T_d$ phase at 600 K; further analysis on the orbital levels of $1T_d$-$MoS_2$; the optimized structures and band gaps of tri-layer $1T_d$-$MoS_2$ with three stacking configurations; AIMD simulations of the temperature-induced phase transition between $1T_d$ phase and 1T phase; the simulated occupied state STM images for 1H, $1T_d$, 1T′ and 1T phases; the total energies and band structures of the other five $MX_2$ monolayers in $1T_d$ phase; computational method for spectroscopic limited maximum efficiency (SLME).

## AUTHOR INFORMATION

**Corresponding Authors**

**yuechen@hku.hk**

**wyc@calypso.cn**

**mym@calypso.cn**

**Notes**

Y. W. and Y. M. designed the research. M. X., F. X., J. L. and Y. W. performed the calculations. M. X., Y. C., Y. W., Z. C. and Y. M. analyzed the results and wrote the manuscript. All authors commented on the manuscript. The authors declare no competing financial interest.

## ACKNOWLEDGEMENTS

M. X., J. L., Y. L., Y. W. and Y. M. acknowledge funding support from the National Natural Science Foundation of China under Grants No. 11474127, No. 11534003, and No.11764043; the National Key Research and Development Program of China under Grant No. 2016YFB0201200, No. 2016YFB0201201, and No. 2016YFB0201204; the 2012 Changjiang Scholars Program of China; supported by Program for JLU Science and Technology Innovative Research Team (JLUSTIRT); and the Science Challenge Project, No. TZ2016001. Y. C. acknowledges funding support from the Research Grants Council of Hong Kong (Grant No. 27202516). Z. C. acknowledges the support from NSF-CREST Center for Innovation, Research and Education in Environmental Nanotechnology (CIRE2N) (Grant Number HRD-1736093) and NASA (Grant 17-EPSCoRProp-0032). Part of the calculation was performed in the high performance computing center of Jilin University and at Tianhe2-JK in the Beijing Computational Science Research Center.

**References**


1. Wang, Q. H., Kalantar-Zadeh, K., Kis, A., Coleman, J. N. & Strano, M. S. Electronics and optoelectronics of two-dimensional transition metal dichalcogenides. *Nat. Nanotechnol.* **7,** 699–712 (2012).
2. Mak, K. F. & Shan, J. Photonics and optoelectronics of 2D semiconductor transition metal dichalcogenides. *Nat. Photonics* **10,** 216–226 (2016).
3. Mak, K. F., Lee, C., Hone, J., Shan, J. & Heinz, T. F. Atomically thin $MoS_2$: A new direct-gap semiconductor. *Phys. Rev. Lett.* **105,** 2–5 (2010).
4. Wu, Z. *et al.* $MoS_2$ nanosheets: A designed structure with high active site density for the hydrogen evolution reaction. *ACS Catal.* **3,** 2101–2107 (2013).
5. Tye, C. T. & Smith, K. J. Catalytic activity of exfoliated $MoS_2$ in hydrodesulfurization, hydrodenitrogenation and hydrogenation reactions. *Top. Catal.* **37,** 129–135 (2006).
6. Chang, K. *et al.* Targeted Synthesis of 2H- and 1T-Phase $MoS_2$ Monolayers for Catalytic Hydrogen Evolution. *Adv. Mater.* **28,** 10033–10041 (2016).
7. Tang, Q. & Jiang, D. E. Mechanism of Hydrogen Evolution Reaction on 1T-$MoS_2$ from First Principles. *Acs Catal.* **6,** 4953–4961 (2016).
8. Zong, X. *et al.* Enhancement of photocatalytic $H_2$ evolution on CdS by loading $MoS_2$ as cocatalyst under visible light irradiation. *J. Am. Chem. Soc.* **130,** 7176–7177 (2008).
9. Voiry, D. *et al.* Conducting $MoS_2$ nanosheets as catalysts for hydrogen evolution reaction. *Nano Lett.* **13,** 6222–6227 (2013).
10. Ganatra, R. & Zhang, Q. Few-layer $MoS_2$: A promising layered semiconductor. *ACS Nano* **8,** 4074–4099 (2014).
11. Zibouche, N., Philipsen, P., Kuc, A. & Heine, T. Transition-metal dichalcogenide bilayers: Switching materials for spintronic and valleytronic applications. *Phys. Rev. B* **90,** 125440 (2014).
12. Singh, E., Kim, K. S., Yeom, G. Y. & Nalwa, H. S. Atomically thin-layered molybdenum disulfide ($MoS_2$) for bulk-heterojunction solar cells. *ACS Appl. Mater. Interfaces* **9,** 3223–3245 (2017).
13. Xu, Z. *et al.* Monolayer $MoS_2$/GaAs heterostructure self-driven photodetector with extremely high detectivity. *Nano Energy* **23,** 89–96 (2016).
14. Tsai, M.-L. *et al.* Monolayer $MoS_2$ Heterojunction Solar Cells. *ACS Nano* **8,** 8317–8322 (2014).
15. Lin, S. *et al.* Interface designed $MoS_2$/GaAs heterostructure solar cell with sandwich stacked hexagonal boron nitride. *Sci. Rep.* **5,** 15103 (2015).
16. Pradhan, S. K., Xiao, B. & Pradhan, A. K. Enhanced photo-response in p-Si/$MoS_2$ heterojunction-based solar cells. *Sol. Energy Mater. Sol. Cells* **144,** 117–127 (2016).

17. Rao, C. N. R. & Maitra, U. Inorganic Graphene Analogs. *Annu. Rev. Mater. Res.* **45,** 29–62 (2015).
18. Yu, Y. *et al.* High phase-purity 1T′-$MoS_2$- and 1T′-$MoSe_2$-layered crystals. *Nat. Chem.* **1**, (2018). doi:10.1038/s41557-018-0035-6
19. Qian, X., Liu, J., Fu, L. & Li, J. Quantum spin Hall effect in two-dimensional transition metal dichalcogenides. *Science,* **346,** 1344–1347 (2014).
20. Ma, F. *et al.* Predicting a new phase (T″) of two-dimensional transition metal di-chalcogenides and strain-controlled topological phase transition. *Nanoscale* **8,** 4969–4975 (2016).
21. Bernardi, M., Palummo, M. & Grossman, J. C. Extraordinary sunlight absorption and one nanometer thick photovoltaics using two-dimensional monolayer materials. *Nano Lett.* **13,** 3664–3670 (2013).
22. Britnell, L. *et al.* Strong Light-Matter Interactions in Heterostructures of Atomically Thin Films. *Science,* **340,** 1311–1314 (2013).
23. Wang, Y. & Ma, Y. Perspective: Crystal structure prediction at high pressures. *J. Chem. Phys.* **140,** 040901 (2014).
24. Wang, Y., Lv, J., Zhu, L. & Ma, Y. Crystal structure prediction via particle-swarm optimization. *Phys. Rev. B* **82,** 094116 (2010).
25. Wang, Y., Lv, J., Zhu, L. & Ma, Y. CALYPSO: A method for crystal structure prediction. *Comput. Phys. Commun.* **183,** 2063–2070 (2012).
26. Wang, Y. *et al.* Materials discovery via CALYPSO methodology. *J. Phys. Condens. Matter* **27,** 203203 (2015).
27. Wang, Y. *et al.* An effective structure prediction method for layered materials based on 2D particle swarm optimization algorithm. *J. Chem. Phys.* **137,** 224108 (2012).
28. Zhu, L. *et al.* Substitutional Alloy of Bi and Te at High Pressure. *Phys. Rev. Lett.* **106,** 145501 (2011).
29. Zhu, L., Liu, H., Pickard, C. J., Zou, G. & Ma, Y. Reactions of xenon with iron and nickel are predicted in the Earth's inner core. *Nat. Chem.* **6,** 644 (2014).
30. Xu, M. *et al.* Anatase (101)-like Structural Model Revealed for Metastable Rutile $TiO_2$ (011) Surface. *ACS Appl. Mater. Interfaces* **9,** 7891–7896 (2017).
31. Lv, J., Wang, Y., Zhu, L. & Ma, Y. Predicted Novel High-Pressure Phases of Lithium. *Phys. Rev. Lett.* **106,** 015503 (2011).
32. Li, Y., Hao, J., Liu, H., Li, Y. & Ma, Y. The metallization and superconductivity of dense hydrogen sulfide. *J. Chem. Phys.* **140,** 174712 (2014).
33. Wang, H., Tse, J. S., Tanaka, K., Iitaka, T. & Ma, Y. Superconductive sodalite-like clathrate calcium hydride at high pressures. *Proc. Natl. Acad. Sci.* **109,** 6463–6466 (2012).
34. Perdew, J. P., Burke, K. & Ernzerhof, M. Generalized Gradient Approximation Made Simple.

*Phys. Rev. Lett.* **77,** 3865–3868 (1996).

35. Kresse, G. & Furthmüller, J. Efficient iterative schemes for ab initio total-energy calculations using a plane-wave basis set. *Phys. Rev. B* **54,** 11169–11186 (1996).
36. Kresse, G. & Joubert, D. From ultrasoft pseudopotentials to the projector augmented-wave method. *Phys. Rev. B* **59,** 1758–1775 (1999).
37. Parlinski, K., Li, Z. & Kawazoe, Y. First-Principles Determination of the Soft Mode in Cubic $ZrO_2$. *Phys. Rev. Lett.* **78,** 4063–4066 (1997).
38. Togo, A., Oba, F. & Tanaka, I. First-principles calculations of the ferroelastic transition between rutile-type and $CaCl_2$-type $SiO_2$ at high pressures. *Phys. Rev. B* **78,** 134106 (2008).
39. Yu, L. & Zunger, A. Identification of potential photovoltaic absorbers based on first-principles spectroscopic screening of materials. *Phys. Rev. Lett.* **108,** 068701 (2012).
40. Heyd, J., Scuseria, G. E. & Ernzerhof, M. Hybrid functionals based on a screened Coulomb potential. *J. Chem. Phys.* **118,** 8207–8215 (2003).
41. Walle, H. P. and C. G. Van de. First-principles study of van der Waals interactions in $MoS_2$ and $MoO_3$. *J. Phys. Condens. Matter* **26,** 305502 (2014).
42. Chhowalla, M. *et al.* The chemistry of two-dimensional layered transition metal dichalcogenide nanosheets. *Nat. Chem.* **5,** 263–275 (2013).
43. Griffith, J. S. & Orgel, L. E. Ligand-field theory. *Quart. Rev. Chem. Soc.* **11,** 381–393 (1957).
44. Kuc, A., Zibouche, N. & Heine, T. Influence of quantum confinement on the electronic structure of the transition metal sulfide $TS_2$. *Phys. Rev. B* **83,** 245213 (2011).
45. Green, M. A., Emery, K., Hishikawa, Y. & Warta, W. Solar cell efficiency tables (version 37). *Prog. Photovoltaics Res. Appl.* **19,** 84–92 (2011).
46. Shah, A. Photovoltaic Technology: The Case for Thin-Film Solar Cells. *Science,* **285,** 692–698 (1999).
47. Takamoto T, Ikeda E, Kurita H, et al. Two-terminal monolithic $In_{0.5}Ga_{0.5}P$/GaAs tandem solar cells with a high conversion efficiency of over 30%. Jpn. J. Appl. Phys. **36**, 6215 (1997)
48. Wang, Y. *et al.* Structural phase transition in monolayer $MoTe_2$ driven by electrostatic doping. *Nature* **550,** 487–491 (2017).
49. Gao, G. *et al.* Charge Mediated Semiconducting-to-Metallic Phase Transition in Molybdenum Disulfide Monolayer and Hydrogen Evolution Reaction in New 1T′ Phase. *J. Phys. Chem. C* **119,** 13124–13128 (2015).
50. Heising, J. & Kanatzidis, M. G. Exfoliated and Restacked $MoS_2$ and $WS_2$ : Ionic or Neutral Species? Encapsulation and Ordering of Hard Electropositive Cations. *J. Am. Chem. Soc.* **121,** 11720–11732 (1999).
51. Hong, J. *et al.* Direct Imaging of Kinetic Pathways of Atomic Diffusion in Monolayer Molybdenum Disulfide. *Nano Lett.* **17,** 3383–3390 (2017).

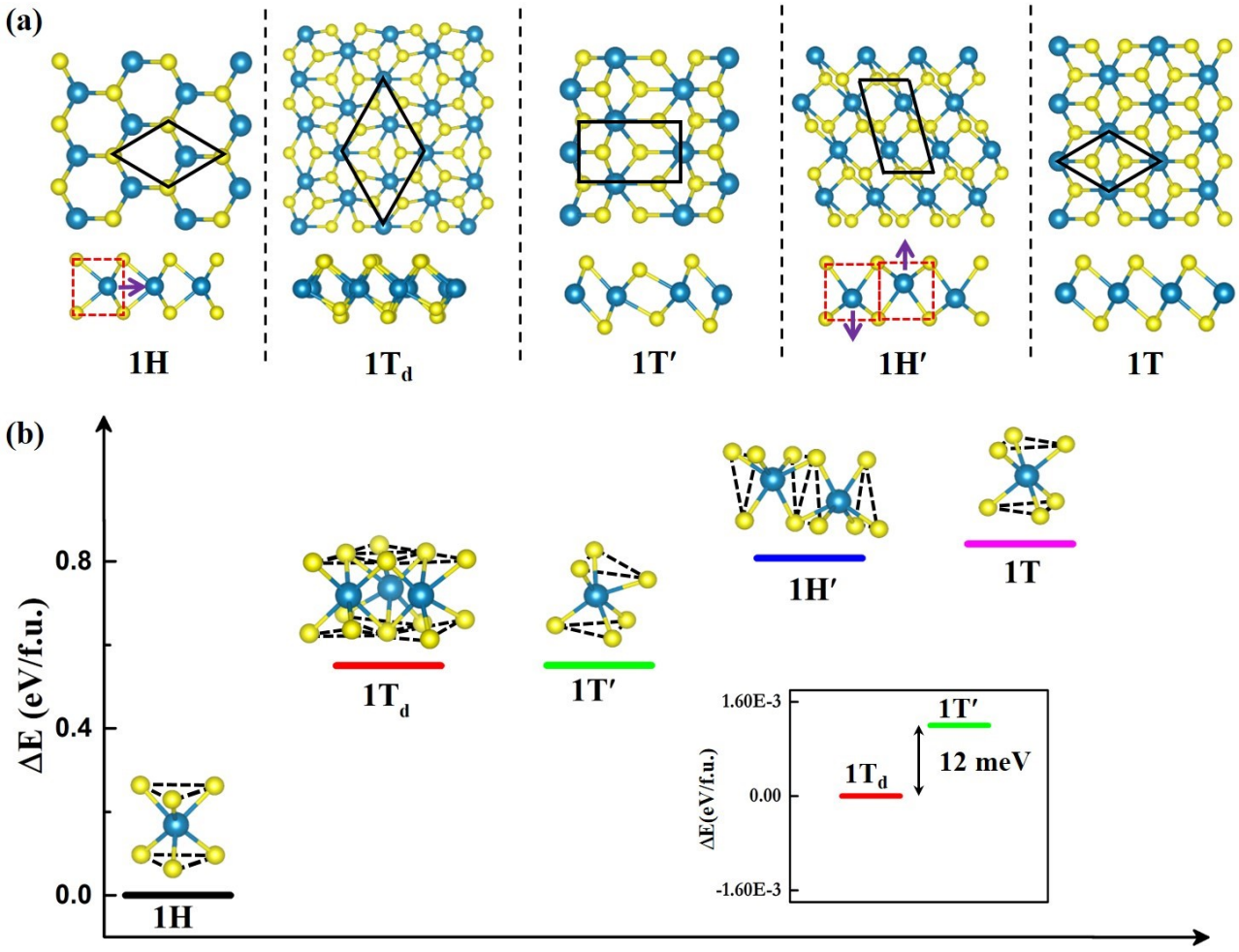


Figure 1. (a) Atomic structures of monolayer $MoS_2$ in 1H, $1T_d$, 1T′, 1H′, and 1T phases. The unit cells are indicated by black solid lines. (b) The calculated total energies (per $MoS_2$ formula unit relative to 1H phase) and the basic building blocks.

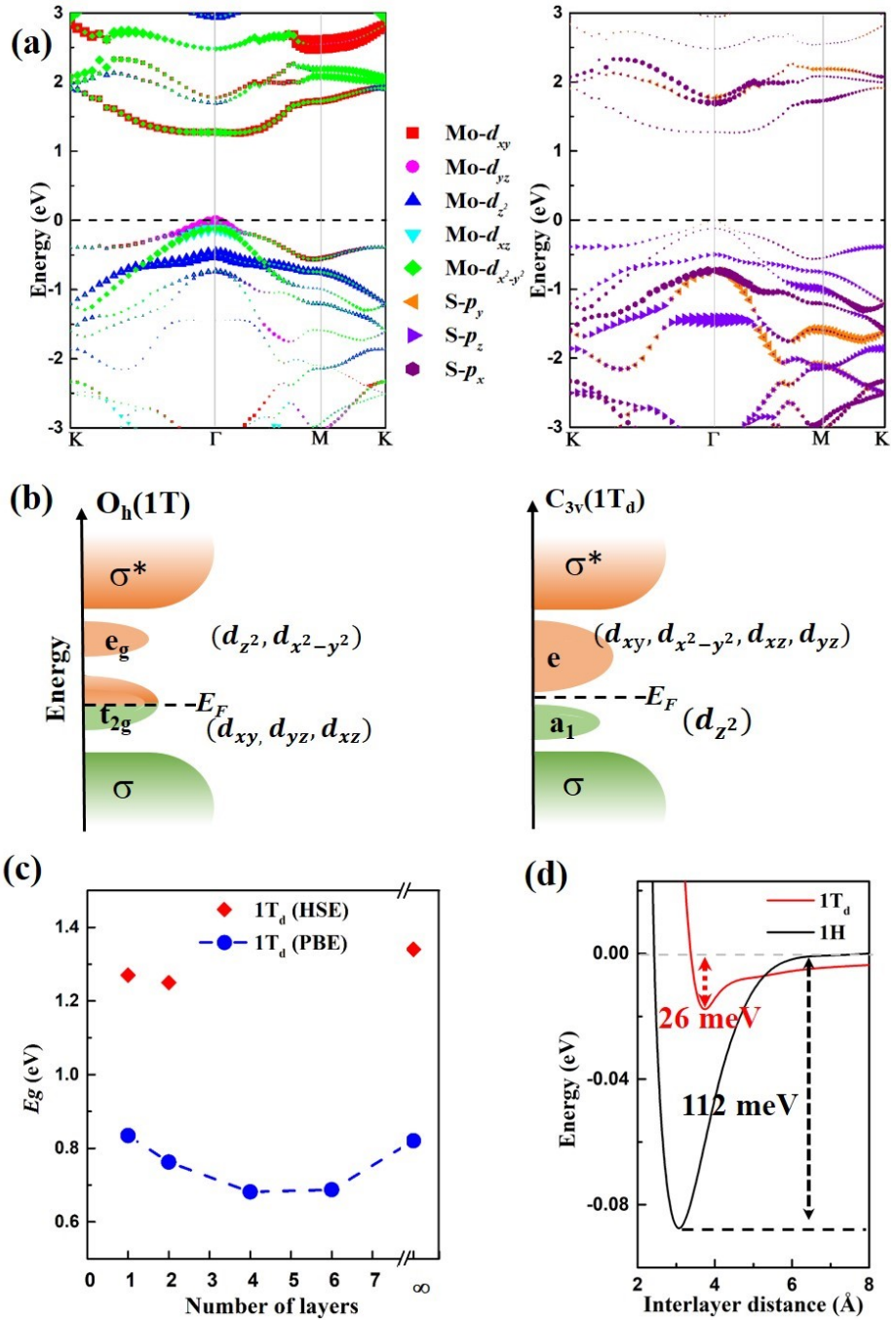


Figure 2. (a) Projected band structure of 1T$_d$-$MoS_2$ phase for Mo atoms (left) and S atoms (right) at HSE level. (b) Schematic illustration showing the progressive filling of d orbitals that are located within the band gap of bonding (σ) and anti-bonding states (σ$^*$) in $MoS_2$. (c) Calculated band gap ($E_g$) as a function of number of layers. (d) The coupling energy of the system as a function of interlayer separation. The different *d*-orbital splitting in crystal structures with octahedral (1T) and distorted octahedral (1T$_d$) geometries. $O_h$ and $C_{3v}$ refer to the point groups associated with the 1T and 1T$_d$ phases, respectively. The filled and unfilled states are shaded with green and light orange, respectively.

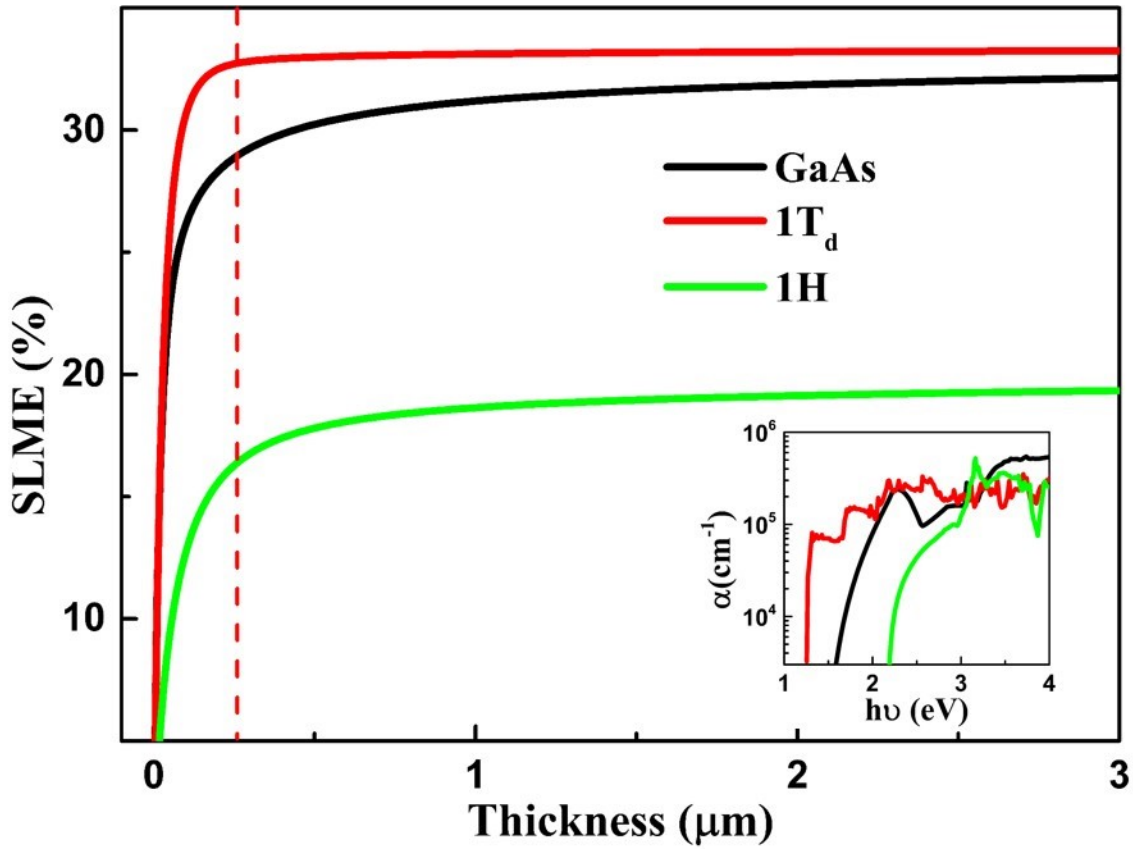


**Figure 3.** SLME as a function of slab thickness for $1T_d$ phase compared with 1H-$MoS_2$ and GaAs. The inset shows their adsorption spectra.

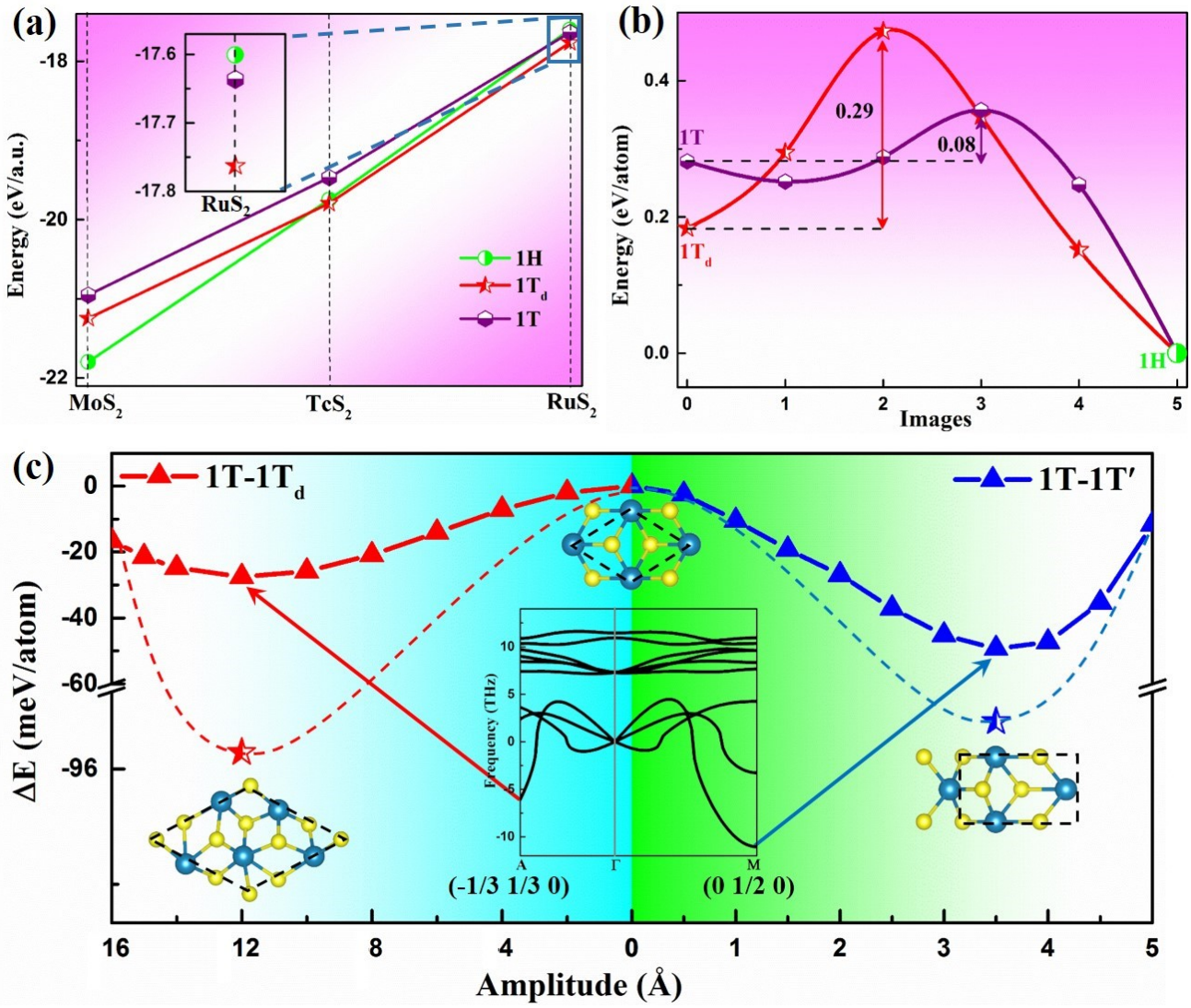


**Figure 4.** (a) The calculated static energies for $MoS_2$, $TcS_2$, and $RuS_2$ in 1H, $1T_d$, and 1T phases. (b) Relative energies to the 1H phase of different images on minimum energy path from $1T_d$ (1T) to 1H phase. (c) The calculated energy as a function of the soft phonon mode amplitudes. On the basis of the eigenvector of the soft mode, we distorted the original 1T $MoS_2$ and then fully optimized the structure, which eventually leads to $1T_d$ (red star) and 1T′ (blue star). The inset shows the phonon dispersions of 1T phase.